1992

(2)

A NUMERICAL SIMULATION OF TWO-PHASE JET SPREADING USING AN EULER-LAGRANGIAN TECHNIQUE

F. Bonetto, D. Drew, R.T. Lahey, Jr.

Center for Multiphase Research

Rensselaer Polytechnic Institute

Troy, NY 12180-3590 USA

The objective of this paper is to study the spreading of a submerged two-phase jet. A plunging liquid jet impacting on a still liquid pool may carryunder bubbles by entraining the surrounding gas. For low liquid jet turbulence, the measured average bubble size was about 200 m [Bonetto and Lahey, 1992]. For low void fraction, one may assume that the liquid velocity field is not disturbed by the presence of the bubbles. This allows the use of known solutions for the velocity field in a planar liquid jet. That is the liquid flow may be solved using Eulerian coordinates and neglecting the effect of the bubbles. The momentum equation for the bubbles has been written in Lagrangian coordinates. The resulting equations are solved for bubble trajectories in the known liquid velocity field.

INTRODUCTION

The gas entrapment by a plunging liquid jet and the resultant two-phase jet dispersion occur in many problems of practical interest. The ecological balance in lakes and oceans is dependent on the amount of dissolved oxygen. In addition, the air carryunder that occurs at most hydraulic structures in rivers is primarily responsible for the large air/water mass transfer that is associated with these structures [Avery and Novak, 1978]. Also, the absorption of CO_2 by the oceans appears to play an important role (as a sink term) in reducing the magnitude of the "greenhouse effect". The absorption of greenhouse gases has been hypothesized to be highly dependent upon the air carryunder that occurs due to breaking waves.

Plunging jets are also used for dissolving gas into liquid. Some chemical reactors use a plunging jet to entrain bubbles, the reaction rate is increased because of the increase in interfacial area and the enhancement in the mass transfer characteristics produced by the turbulence in the two-phase jet.

The problem under study is a planar liquid jet impacting on a liquid pool surrounded by a still gas. Lezzi and Prosperetti [1991] and Bonetto et al [1992] have recently proposed mechanisms for the gas entrainement. In this work the dispersion of a two-phase jet is studied. A dilute dispersion of bubbles in the liquid is assumed. The liquid velocity field is assumed to not be affected by the presence of the bubbles. The momentum balance equations are presented in the Momentum Balance Section. Then, the Tolmien's solution for the mean velocity of a turbulent liquid jet is derived. Finally, the integrated bubble trajectories and other derived quantities of interest, such as the maximum penetration depth of the bubble, the total time that the bubbles are under water and their emergence position at the pool's surface are presented.

MOMENTUM BALANCE

Newton's law for the gas phase takes the form

$$\rho_g V_g \frac{D_g \underline{u}_g}{Dt} = \underline{F} \qquad (1)$$

where $_g$, V_b, $\underline{u}_g$ are the particle density, volume and velocity, respectively. $\frac{D_g \underline{u}_g}{Dt}$ is the material derivative of the particle velocity following the particle and $\underline{F}$ is the applied force.

It is convenient to divide the force, $\underline{F}$, into three parts, one being the inviscid flow force (Re=∞) and the others corresponding to viscous flows F_V and the buoyancy force F_B.

$$\underline{F} = \underline{F}_I + \underline{F}_V + \underline{F}_B \qquad (2)$$

i) Inviscid flow force: The inviscid flow force can be further separated into two parts, one corresponding to an irrotational flow and the other corresponding to a rotational flow.

$$\underline{F}_I = \underline{F}_I^{(irrot)} + \underline{F}_I^{(rot)} \tag{3}$$

For spherical bubbles in inviscid irrotational flows the force $\underline{F}_I$, assuming that the liquid phase pressure gradient is impressed on the bubbles, is given by:

$$\underline{F}_I^{(irrot)} = \rho_\ell V_b \left[(1 + C_{vm}) \frac{D_\ell \underline{u}_\ell}{Dt} - C_{vm} \frac{D_g \underline{u}_g}{Dt} \right] \tag{4}$$

where $\underline{u}_\ell$ is the liquid velocity, $\frac{D_\ell \underline{u}_\ell}{Dt}$ is the material derivative following the liquid and C_{vm} is the virtual mass coefficient (for spheres C_{vm}=1/2). The term $\frac{\partial \underline{u}_\ell}{\partial t}$ is zero because in this study the liquid flow was steady, thus the liquid acceleration is given by,

$$\frac{D_\ell \underline{u}_\ell}{Dt} = (u_\ell \bullet \nabla)\underline{u}_\ell$$

A general expression has been derived for the lateral force on a sphere in weakly rotational flows ($\nabla \underline{u}_\ell \neq 0, \frac{|\nabla \underline{u}_\ell| R_b}{|u_r|} << 1$). Auton et al [1988] and Drew & Lahey [1987,1990] show that,

$$\underline{F}_I^{(rot)} = C_L (\underline{u}_g - \underline{u}_\ell) \times \nabla \times \underline{u}_\ell \tag{5}$$

where C_L is the lift coefficient which, for spheres is, C_L=1/2.

ii) Viscous Flows (moderate Re): The effect of the viscous stress will now be considered. A particle moving in a steady flow has a non-steady component of the drag force due to vortex shedding. The viscous force is then:

$$\underline{F}_V(t) = \underline{F}_D + \underline{F}_\perp(t) \tag{6}$$

$$\underline{F}_D = \frac{1}{2}\rho_l C_D A_b |\underline{u}_r| \underline{u}_r \tag{7}$$

Where $\underline{F}_D$ is the steady drag force component parallel to the relative velocity and $\underline{F}_\perp(t)$ is the non steady force component perpendicular to the relative motion. For moderate Re numbers (Re $\cong$ 100) the drag force is caused by the pressure field asymmetry in the flow around the particle. The vortex shedding produces an oscillating pressure distribution around the bubble and a non-steady force component. Graham [1980] showed that if the Strouhal number is $S=R_b/(|u_r| T) < 0.3$, $\underline{F}_\perp(t)$ is less than 10 % of the value of $\underline{F}_D$, where T is the period of the vortex shedding. In our simulation the previous condition is satisfied and hence $\underline{F}_\perp(t)$ is neglected. That is,

$$\underline{F}_V \cong \underline{F}_D \tag{8}$$

iii) Buoyancy force: The buoyancy force is due to the difference in density between the bubbles and the liquid,

$$\underline{F}_B = (\rho_\ell - \rho_g) V_b \underline{g} \tag{9}$$

Finally, we note that,

$$\frac{D_g \underline{x}_g}{Dt} = \underline{u}_g \tag{10}$$

where $\underline{x}$ is the position of the particle at time t. The momentum balance equation is obtained by combining Eqs. (1) to (5), (8) and (9). It is convenient to write Eq. (10) and the momentum balance in component form for a two-dimensional steady-state flow:

$$\frac{D_g y_g}{Dt} = u_{gy} \tag{11a}$$

$$\frac{D_g z_g}{Dt} = u_{gz} \tag{11b}$$

$$\rho_g V_b \frac{D_g \underline{u}_g}{Dt} = \rho_\ell V_b (\underline{u}_\ell \bullet \nabla)\underline{u}_\ell + C_{vm}\rho_\ell V_b \left[(\underline{u}_\ell \bullet \nabla)\underline{u}_\ell - \frac{D_g \underline{u}_g}{Dt} \right]$$

$$\tfrac{1}{2}\rho_\ell A_b C_D |\underline{u}_\ell - \underline{u}_g|(\underline{u}_\ell - \underline{u}_g) + (\rho_\ell - \rho_g)V_b \underline{g}$$

$$+ C_L \rho_\ell V_b \underline{u}_r \times (\nabla \times \underline{u}_\ell) \tag{11c}$$

TOLMIEN SOLUTION

Let us now consider the solution for a spreading turbulent single-phase liquid jet. The jet has a uniform velocity profile where it impacts the liquid pool at z=0. After the impact, a boundary layer develops at the edge of the jet. Figure-1 shows the different jet regions. Region-1 is the inviscid core. Inside this region the velocity is the inlet velocity, V. Region-2 is where the jet is approximately self-similar. At larger distances from the impacting point the jet is closer to a true self-similar condition. Tolmien's calculation will be followed to obtain [Hinze, 1975] the mean velocity values in the self-similar region. It is assumed that the liquid emanates from an infinitely narrow cross section. Also it is assumed that the pressure inside the jet is uniform and equal to the surrounding pressure. Then the momentum crossing a plane perpendicular to the direction of the flow is constant:

$$\int_0^\delta \rho u_2^2 dy = \text{constant} \tag{12}$$

Assuming the velocity profile is self-similar,

$$\frac{u_z}{u_z^0} = f(\frac{y}{z'}), \quad \text{then} \quad \int_0^{b/z'} (\frac{u_z}{u_z^0})^2 \frac{dy}{z'} = \text{constant} \tag{13}$$

where z' is the axial distance measured from the infinitely narrow cross section. Combining eqs. 12 and 13 we obtain the relationship between the center-line axial velocity uz(y=0) and z' is as:

$$u_z^0 = u_z(y=0) = \frac{c}{\sqrt{z'}} \tag{14}$$

where c is a constant. The velocity at an arbitrary point is given by:

$$u_z = \frac{c}{\sqrt{z'}} f(\eta) \tag{15}$$

It is useful to define the stream function as:

$$u_z = \frac{\partial \psi}{\partial y} \quad u_y = -\frac{\partial \psi}{\partial z} \tag{16}$$

then

$$\psi = \int u_z dy = c\sqrt{z'} F(\eta) \quad \text{, where,}$$
$$F(\eta) = \int f(\eta) d\eta \tag{17}$$

The momentum balance in the z direction for the control volume shown in Figure-1 is:

$$u_z u_y + \frac{\partial}{\partial z'} \int_{\infty}^{y} u_z^2 dy + d^2 z'^2 \left(\frac{\partial u_z}{\partial y} \right)^2 = 0 \tag{18}$$

where d is the mixing length constant and, according to mixing length theory, the turbulent shear stress was assumed to be,

$$\tau = -\rho d^2 z'^2 \left(\frac{\partial u_z}{\partial y} \right)^2 \tag{19}$$

Using Eqs. (16) and (17) we obtain:

$$2d^2 (F''(\eta))^2 = F(\eta) F'(\eta) \tag{20}$$

Introducing the additional change of variables,

$$\varphi = \frac{\eta}{a} \quad \text{, where,} \quad a = \sqrt[3]{(2d^2)} \tag{21}$$

yields,

$$(F''(\varphi))^2 = F(\varphi) F'(\varphi) \tag{22}$$

The appropriate boundary conditions at the centerplane φ=0 are that the lateral velocity u_y equals zero and the axial velocity u_z is u_z(y=0), thus,

$$F(\varphi = 0) = 0 \quad , \quad F'(\varphi = 0) = 1 \tag{23}$$

Equation (22) has been numerically integrated with the boundary conditions Eq. (23). In order to compute the velocities the value of the parameter has to be known. The value obtained experimentally by Forthmann [Abramovich, 1963] was used, that is, a=0.11.

Note that this calculation corresponds to a jet that is self-similar everywhere and that it emerges from an infinitely narrow slit. Actually, the jet emerges from a finite slit with half width equal to h and constant velocity V. In order to reconcile these differences an effective origin is computed for the Tolmien jet, and it is required that its momentum agree with the actual jet momentum at impact. The momentum flux conservation condition is:

$$\rho_\ell \int_o^\delta u_z^2 dy = \rho_\ell V^2 h \qquad (24)$$

The distance from the infinitely narrow slit, z', and the distance from the finite slit, z, are related by,

z'=z+s ,where, s=0.41h/a

A final modification has to be made to the self-similar solution to account for the inviscid core region. For the infinitely narrow solution the velocities goes to infinity we get closer to the slit. In the finite slit, the velocity can not exceed the inlet velocity V, thus wherever the velocity exceeds V, it is reset to V. Figs. 2 and 3 show the lateral and the axial velocity u_y and u_z as a function of the lateral coordinate y for different axial positions z. Note that at the inlet the velocity profile is uniform and the jet is spreading as we increase the axial position z. Figs. 4 to 8 show the various spatial derivatives.

DRAG LAW

To this point, the analysis is valid for both bubbles and solid particles. However, there is a difference between the drag that the liquid exerts on a bubble compared to that for a solid particle.

The so-called "dirty water" Wallis drag correlation as been used to compute the drag on bubbles:

$$C_D = \frac{6.3}{Re^{0.385}} \qquad (25)$$

In contrast the Clift, Grace and Weber correlation is generally used to compete the drag in liquid/solid flows

$$C_D = \frac{24}{Re}\left(1 + 0.15\,Re^{0.687}\right) + \frac{0.42}{\left[1 + 4.25\,10^4\,Re^{-1.16}\right]} \qquad (26)$$

where $Re=2\ R_s\ |u_r|/\upsilon_\ell$

RESULTS

Before presenting the results is convenient to make the following change of variables:

$$x_1 = y\cos(\theta) + z\sin(\theta)$$

$$x_2 = y\sin(\theta) - z\cos(\theta)$$

Figure 9 shows the trajectories of three bubbles with initial positions (a) ($y=-h/2, z=R_b$), (b) ($y=0, z=R_b$) and (c) ($y=h/2, z=R_b$). Bubble (a) is initially at the center plane, while the other two are initially at one side or the other of the jet centerplane halfway to the edge of the jet. For the case shown in Figure 9, the liquid planar jet is impacting the pool at an angle of $\theta=45$ degrees with respect to the vertical. The uniform velocity of the jet at the impacting point is V=5m/s, the jet width is 2h=4.16 mm and the radius of the bubble is R_b=2mm. For the base case we used the coefficients of the lift force and the virtual mass force computed analytically assuming that the liquid was inviscid, that is, $C_{vm}=1/2$ and $C_L=1/2$.

A qualitative description of the flow follows. We consider first the bubble that is initially at the center of the jet. In the inviscid core region, all derivatives of the liquid velocity field are zero, then the only forces acting acting on the bubbles are drag and buoyancy. The drag force acts on the bubble in the same direction that the liquid flow. In the inviscid core the lateral velocity, u_y, is zero and the axial velocity, u_z, is equal to V. Thus, the drag force in the inviscid core tends to move the bubble parallel to the jet and at a gas velocity near V. The buoyancy force acts in the upward vertical direction. That is, buoyancy tends to cause the bubble to move towards the free surface. In the self-similar region, the lift force keeps the bubble near the centerplane, the virtual mass reduces the acceleration that the bubble experiences for a given force.

We take the previous solution as the base solution in parameter space. Then the effect of the different parameters are explored one at a time and

compared with the base solution.

MAXIMUM DEPTH

One of the important parameters is the maximum depth that a given bubble reaches. Figure 10 shows the maximum depth as a function of the inlet liquid velocity V for three different inlet positions. The increase of the maximum depth with the velocity is easily seen. This is expected because when we increase the velocity by a factor ΔV, the lift force that keeps the bubble near the center plane increases a factor $(\Delta V)^2$ while the buoyancy force that tends to move the bubble toward the free surface remains the same. Notice that the depth reached by bubble with initial conditions in the lower half of the jet have similar trajectories compared to the bubbles initially at the center plane. This is again due to the fact that the bubbles that remain near the centerplane longer are the ones that reach greater depths. A typical trajectory of a bubble that is at the lower half of the jet initially is as follows: buoyancy tends to move it up (i.e. toward the center plane), however as the bubble gets closer to the center plane, the higher liquid velocities there produce a larger drag and the bubble flows toward greater depths.

EMERGENCE DISTANCE

Another quantity of importance is the distance from the jet impact position to the place where the bubble reemerges at the free surface. Figure 11 shows the distance of emergence, s, as a function of the jet inlet velocity V for three different initial bubble positions. Again the s increases with the inlet velocity V because of the effect of the lift force . It is clearly seen in Figure 11 that the bubbles that are initially in the lower half of the jet ($y_i<0$) have a longer emergence distance s than the bubbles initially in the upper half of the jet ($y>0$). Therefore s increases as a function of the initial bubble position y_0 ($-h<y_0<h$). Thus, the larger the initial position y_0 ($-h<y_0<h$), the larger the emergence distance s, except for y_0 very near -h. For y_0 values near -h, an interesting phenomenon occurs. Figure 9 shows two typical trajectories with $y_{0_1}>y_{0_2}$ both in the neighborhood of $y_0 = -h$. The buoyancy force acts over the bubble with initial position y_{0_1} producing a lateral velocity $u_{\ell y} >0$ which

is greater than the lateral velocity of bubble number 2, $u_{y_1} > u_{y_2} > 0$. Then, bubble-1 crosses the jet centerplane sooner than the bubble-2. Thus, bubble 2 has a larger emergence distance s.

Notice that the two trajectories cross each other . An Eulerian approach would give some kind of average behavior at this point. This result does not contradict the fact that a set of Ordinary Differential Equations (ODE) has an unique solution. The trajectories are non-crossing in full phase space. The dimension of the space is equal to the number of independent equations (i.e., four). Thus the coordinates in phase space are y,z,u_y,u_z. The trajectories presented in the y-z plane can be seen as projections of the trajectories in full phase space on the y-z plane. Note that the x_1-x_2 plane is identical to the y-z plane. This effect can not occur using partial differential equations resulting from the Eulerian approach. The corresponding solution would effectively average the different velocities at trajectory crossings, and would result in a single velocity at each point.

SENSITIVITY OF THE SOLUTION TO THE PROBLEM PARAMETERS

We wish to study the effect of the various parameters on the resulting bubble trajectories. What follows is a parametric study of the solution of eq (11). In the following figures the dashed lines correspond to the base solution trajectories from the previous section. The solid lines show the effect of changing the corresponding parameters. Again curves (a), (b) and (c) correspond to the initial conditions described in Fig. 9.

In Figs. 13 and 14, the lift coefficient was varied, with C_L=0.25 (for a base case solution of C_L=0.5). For the trajectories (a) and (b) the reduction in the lift coefficient produces a reduction in the ability of the bubble to remain near the center plane. The y component of the lift force is:

$$F_{Iy}^{(rot)} = C_L(u_{\ell_z} - u_{g_z})\left(\frac{\partial u_{\ell_z}}{\partial y} - \frac{\partial u_{\ell_y}}{\partial z}\right) < 0, \quad \text{if,} \quad y > 0$$

Figure 8 shows the derivatives as a function of y. This factor is always negative for y>0. Also the axial component of the relative velocity is positive. Thus for y>0 the lift force tries to push the bubblea to the centerline. At the center plane the axial liquid velocity has a maximum and therefore the drag acts to move the bubble to greater depths. Obviously, there is a strong dependence of the emergence point, s, on the value of the lift coefficient.

There is also a lift force component in the axial direction:

$$F_{I_z}^{(rot)} = C_L (u_{g_y} - u_{\ell_y}) \left(\frac{\partial u_{\ell_z}}{\partial y} - \frac{\partial u_{\ell_y}}{\partial z} \right)$$

For bubbles in the upper half of the jet, the lateral bubble velocity component is in general greater than the lateral liquid velocity component. Thus, the lift force component in the axial direction is negative. For trajectory (c) the negative lift force component in the z direction is reduced and the emergence position, s, is increased. In Fig 14 the lift force has been completely eliminated (C_L=0) and we find that the emergence distance of the trajectories, s, are fairly close together. Hence we find that a larger lift coefficient results in a spreading of the emergence distance for the various trajectories.

Figs. 14 and 15 correspond to varying the virtual mass coefficient from the base case value of C_{vm} = 0.5, to C_{vm} =0.4 and C_{vm} =1.0. We note that a larger virtual mass coefficient results in less acceleration of the bubble, so that an increase in the virtual mass coefficient produces an increase in the ability of the bubble to follow the liquid flow.

Figs. 16 and 17 corresponds to the effect of the jet inclination angle, θ. Fig. 16 shows a jet impacting at an angle of 40 degrees (base case =45°). The maximum depth d_m is seen to be sensitive to the angle . On the contrary, the location of the emergent bubble is seen to be somewhat insensitive to the angle . Fig. 18 shows a jet impacting at an angle =60 degrees. For this case both the maximum depth, d_m, and the distance of emergence, s, are seen to be strongly affected by the impacting angle.

SUMMARY AND CONCLUSIONS

A dilute bubbly jet has been analyzed using a Eulerian-Lagrangian approach. It is assumed that the presence of the bubbles does not affect the liquid flow. Under this assumption the liquid flow is decoupled from the bubble motion, and is given by the Tollmien self-similar jet solution modified to account for the inviscid core. That is, it was not necessary to solve for the liquid flow field. The momentum balance for the gas phase has been rewritten as a system of four ODEs. The independent variable is time and the four dependent variables are the bubble position (y, z) and the bubble velocity components (u_y, u_z). The system of ODEs was integrated using a fifth order Runge Kutta scheme. The initial conditions were: $y(t=0)=y_0$, $z(t=0)=0$,$u_y(t=0)=0$,$u_y(t=0)=V$.

Based on the computed trajectories, three quantities of practical interest were estimated: The maximum depth d_m, the bubble emergence distance, s, and the total time that the bubble is immersed in the pool, t. One may be interested in knowing the aeration produced by a breaking wave in the sea. The maximum depth provides information about the amount of the aerated layer. The time under water gives information about the amount of gas that is dissolved. However, in order to compute the amount of dissolved gas, an additional model for the diffusion process needs to be included. Finally, the distance of emergence gives information about the horizontal extent of the aeration produced by the breaking of a single wave. The results show that d_m, t and s increase with the jet velocity, with faster increase for low values of V. Also the bubbles initially at the lower half of the jet have larger dm, t and s than the bubbles initially at the upper half of the jet for the same velocity.

The relative velocity in the axial direction, u_{g_z}-u_{ℓ_z} is negative inside the jet. Thus the lateral component of the lift force tends to move the bubble toward the jet centerplane. The axial component of the lift force is negative if the relative velocity is positive and this force tends to retard the bubble motion.

The effect of virtual mass force is not as straightforward to analyze.

The reason is that the terms $\frac{\partial u_{\ell z}}{\partial y}$ and $\frac{\partial u_{\ell y}}{\partial z}$ change sign inside the liquid jet. This can be easily seen in Figs. 4 and 7.

We conclude that both the virtual mass and the lift forces play an important role in the spreading of a two-phase jet.

ACKNOWLEDGMENT

The authors wish to acknowledge the funding provided for this research by the Office of Naval Research (ONR), Grant No N-0001491-J-1271, Fluid Dynamics Program.

REFERENCES

Abramovich, G. "The Theory of Turbulent Jets", MIT Press, (1963).

Avery, S. & Novak, P., "Oxygen Transfer at Hydraulic Structures", Journal of Hyd. Div., ASCE, vol 104 (HY11), pp. 1521-1540, (1978).

Auton, T.R.; Hunt, J.C.R. & Prud'homme, M., "The Force Exerted On A Body In Inviscid Unsteady Non-Uniform Rotational Flow". J. Fluid Mech., 197, pp. 241-257, (1988).

Bonetto, F. and Lahey, R.T.,"An Experimental Study On Air Carryunder Due To A Plunging Liquid Jet". To be published in Int. Journal of Multiphase Flow, (1992).

Drew, D.A. & Lahey, R.T., "The Virtual Mass And Lift Force On A Sphere In Rotating And Straining Inviscid Flow", Int. J. Multiphase Flow, 13, #1, pp.113-121, (1987).

Drew, D.A. & Lahey, R.T., "Some Supplemental Analysis Concerning The Virtual Mass And Lift Force On A Sphere In A Rotating And Straining Flow", Int. J. Multiphase Flow, 16, #6, pp. 1127-1130, (1990).

Graham, J.M.R., "The Force On Sharp-Edged Cylinders In Oscillatory Flow At Low Keulegan-Carpenter Numbers", J. Fluid Mech., 20, pp. 331-346, (1980).

Hinze, J.O., "Turbulence", McGraw-Hill, (1975).

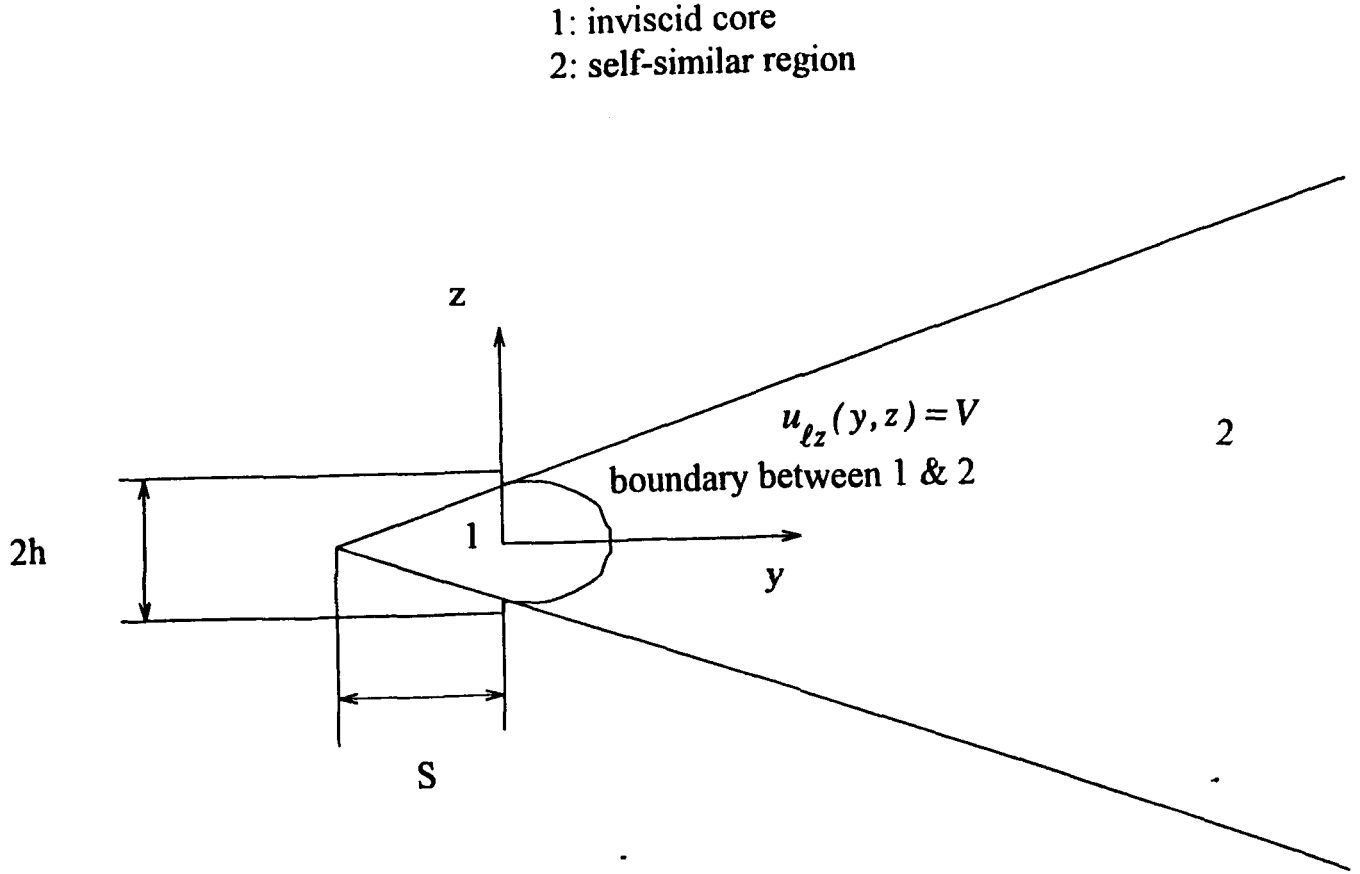

Figure 1: The inviscid and self similar regions of a planar jet

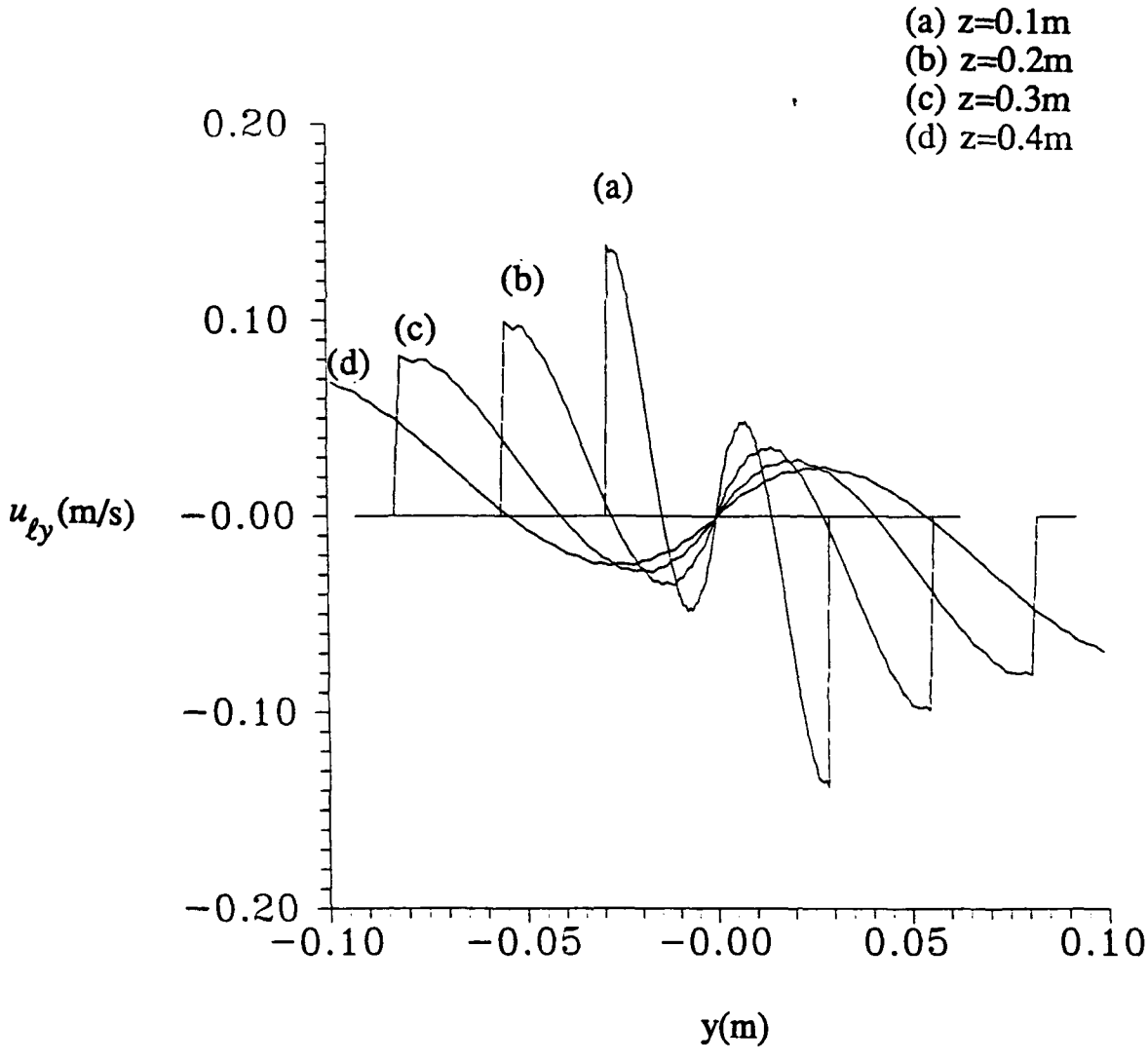

Figure 2: Lateral velocity $u_{\ell y}$ as a function of the lateral position y for different axial positions z

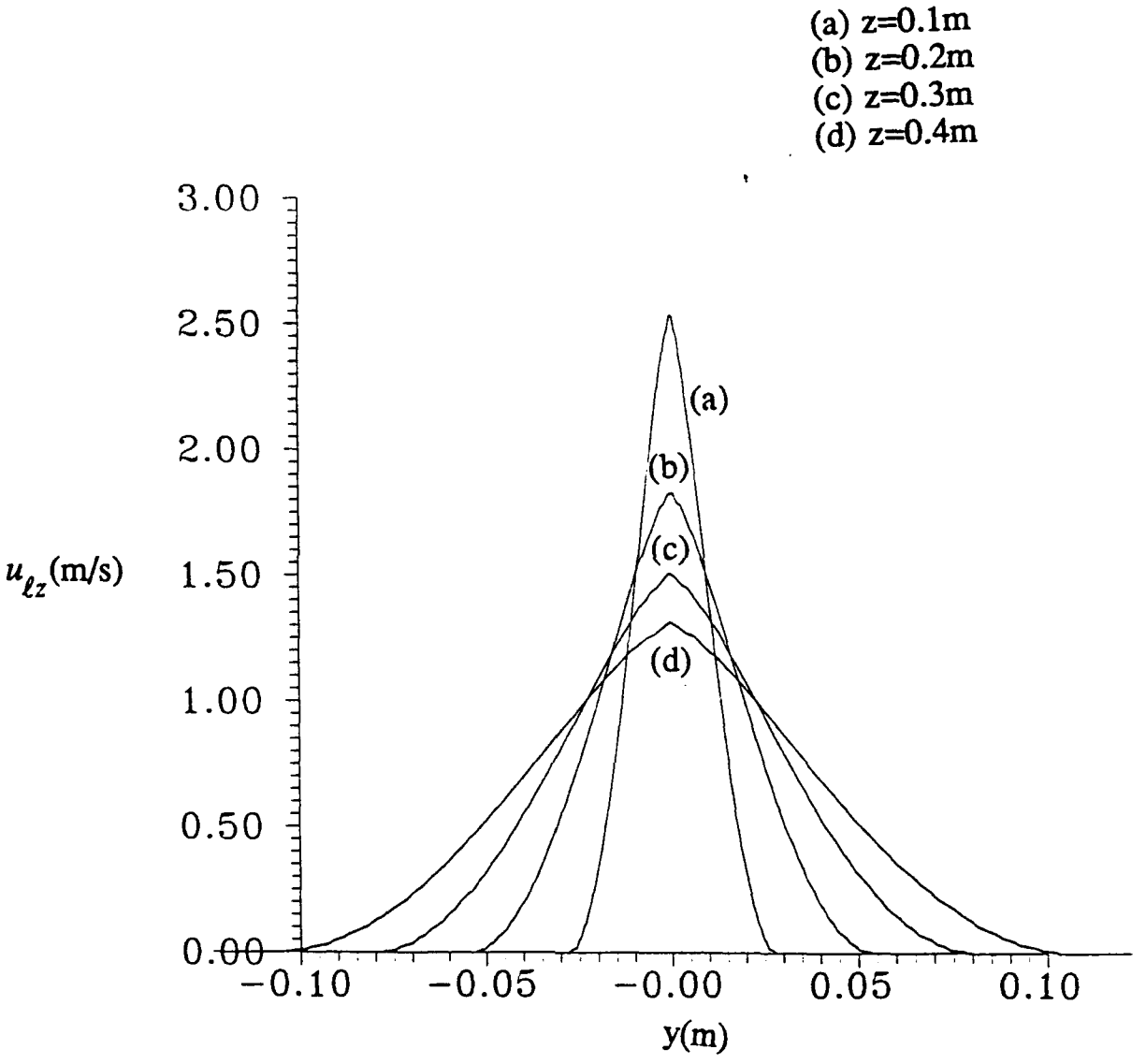

Figure 3: Axial liquid velocity $u_{\ell z}$ as a function of the lateral position y for different axial positions z

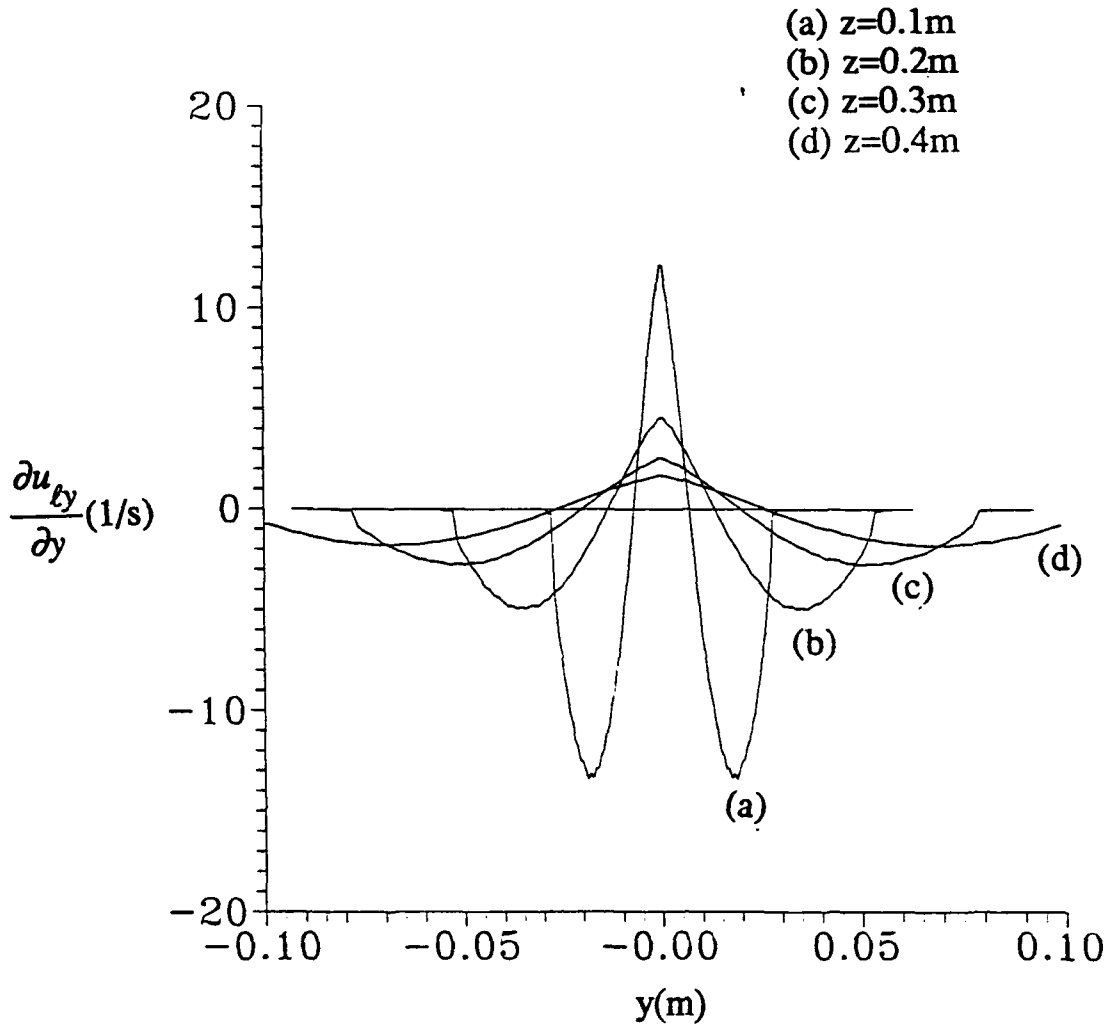

Figure 4: $\frac{\partial u_{\ell y}}{\partial y}$ as a function of the lateral position y for different axial positions z

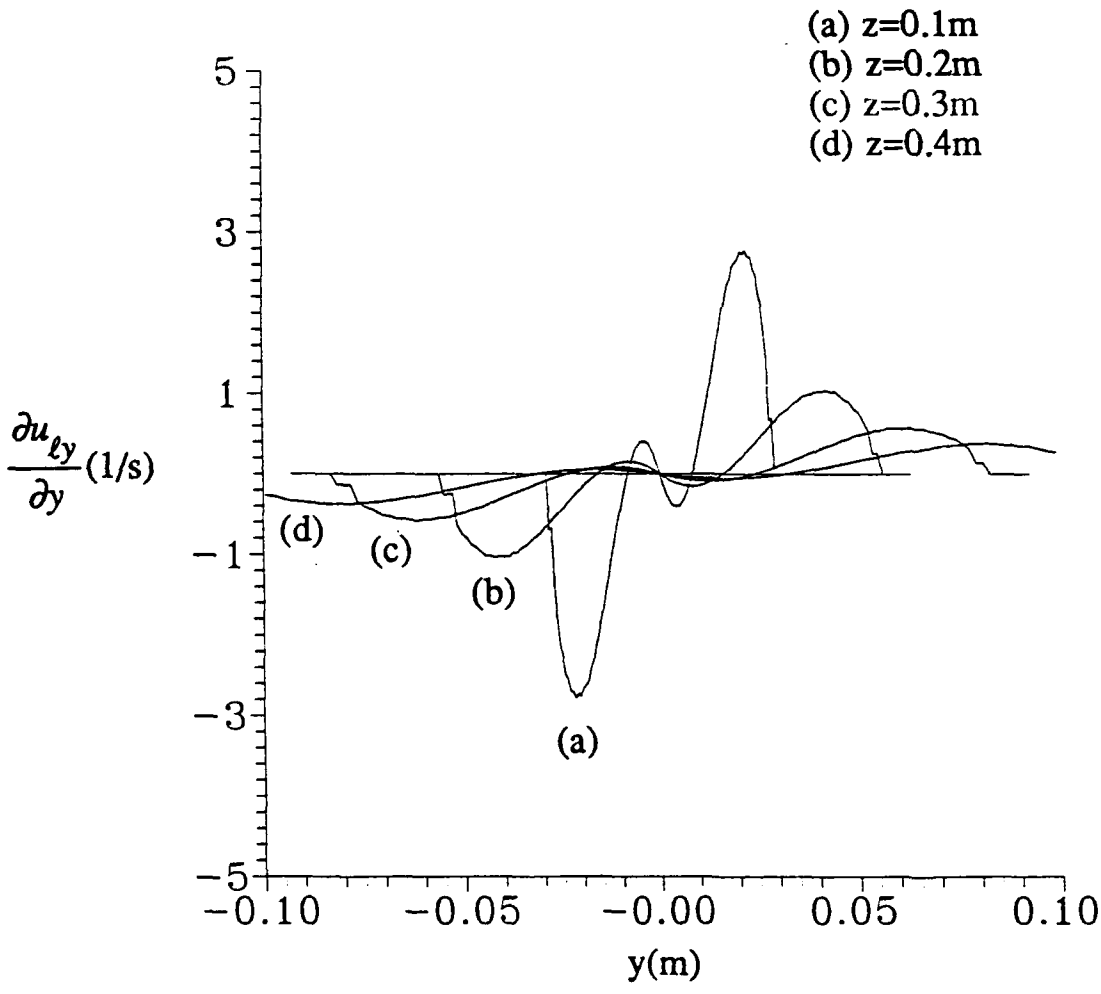

Figure 5: $\frac{\partial u_{\ell y}}{\partial z}$ as a function of the lateral position y for different axial positions z

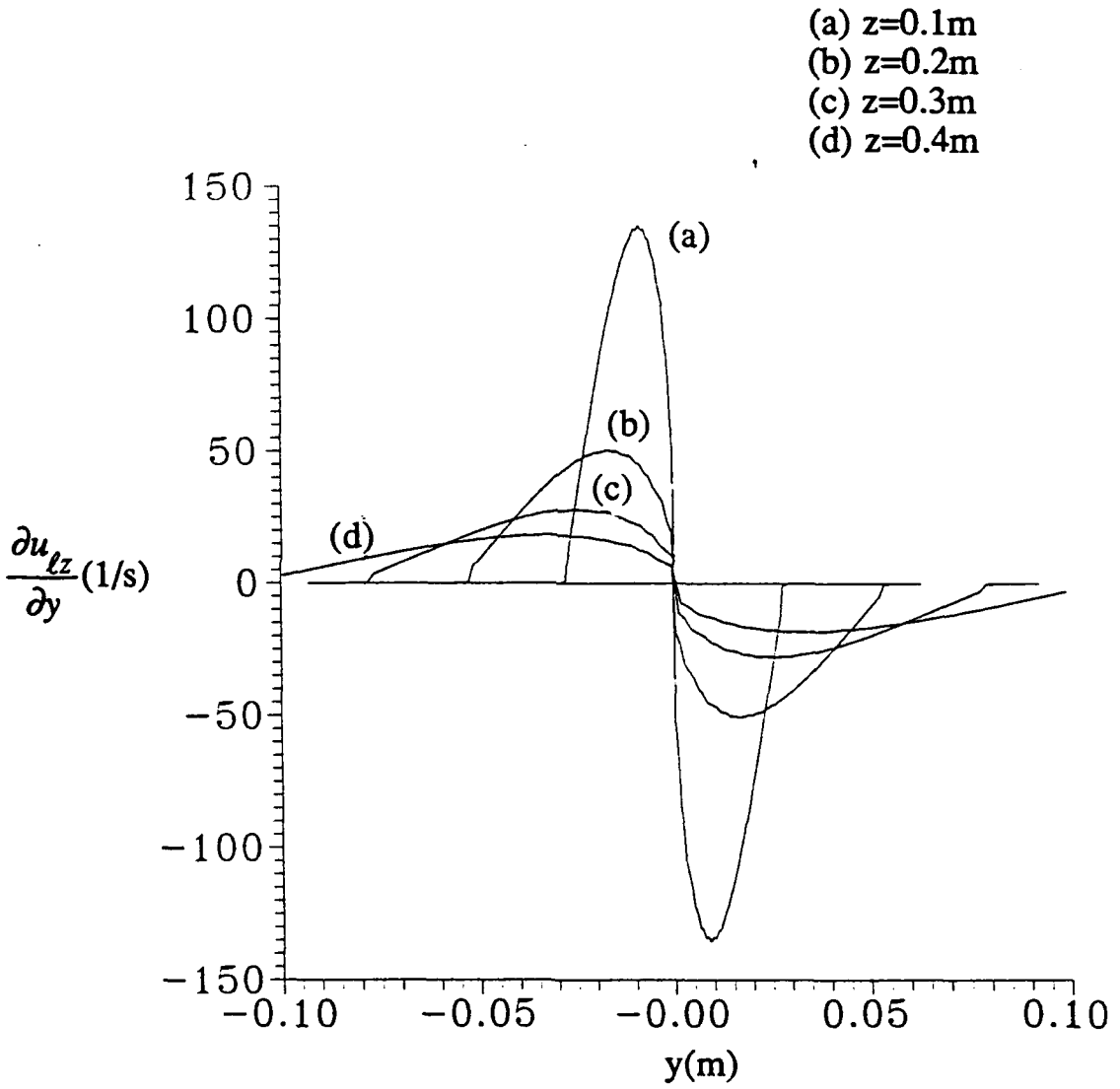

Figure 6: $\frac{\partial u_{\ell z}}{\partial y}$ as a function of the lateral position y for different axial positions z

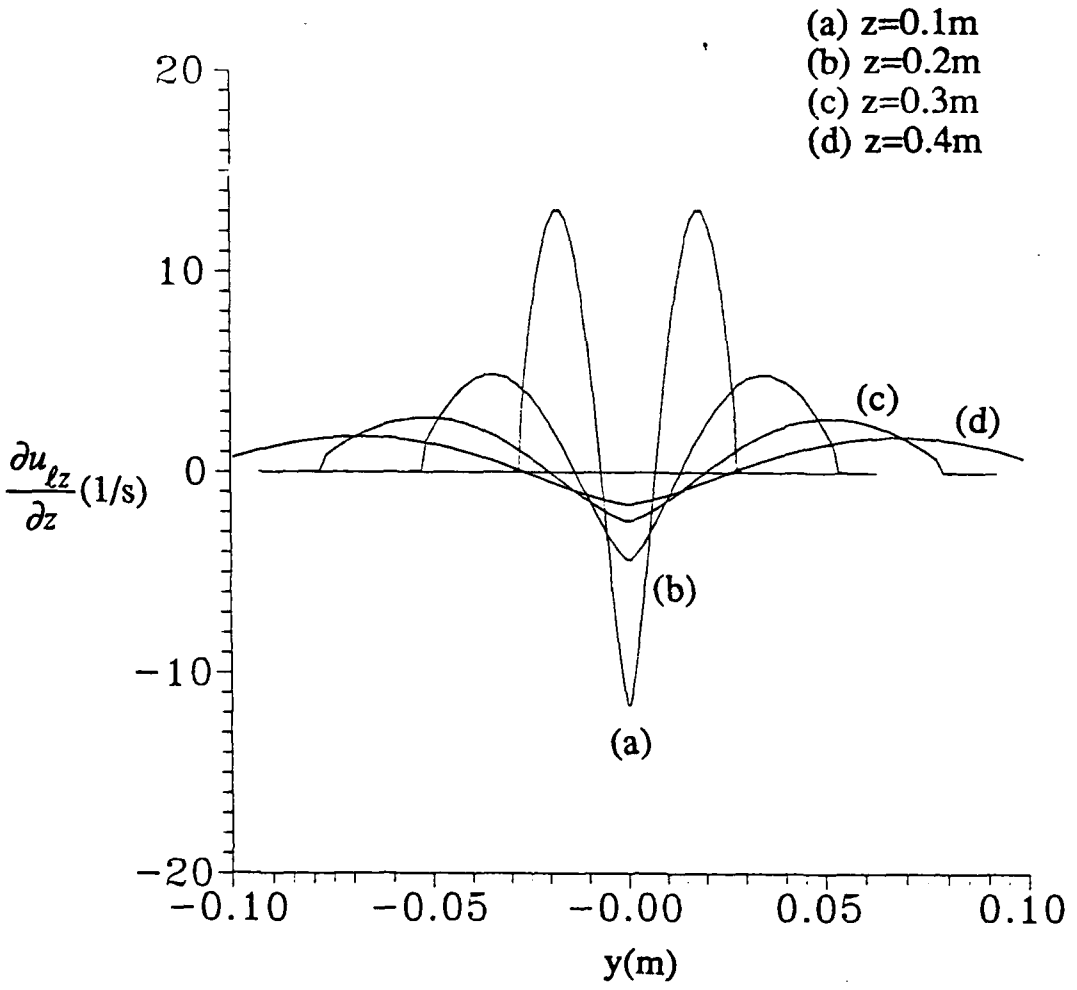

Figure 7: $\frac{\partial u_{\ell z}}{\partial z}$ as a function of the lateral position y for different axial positions z

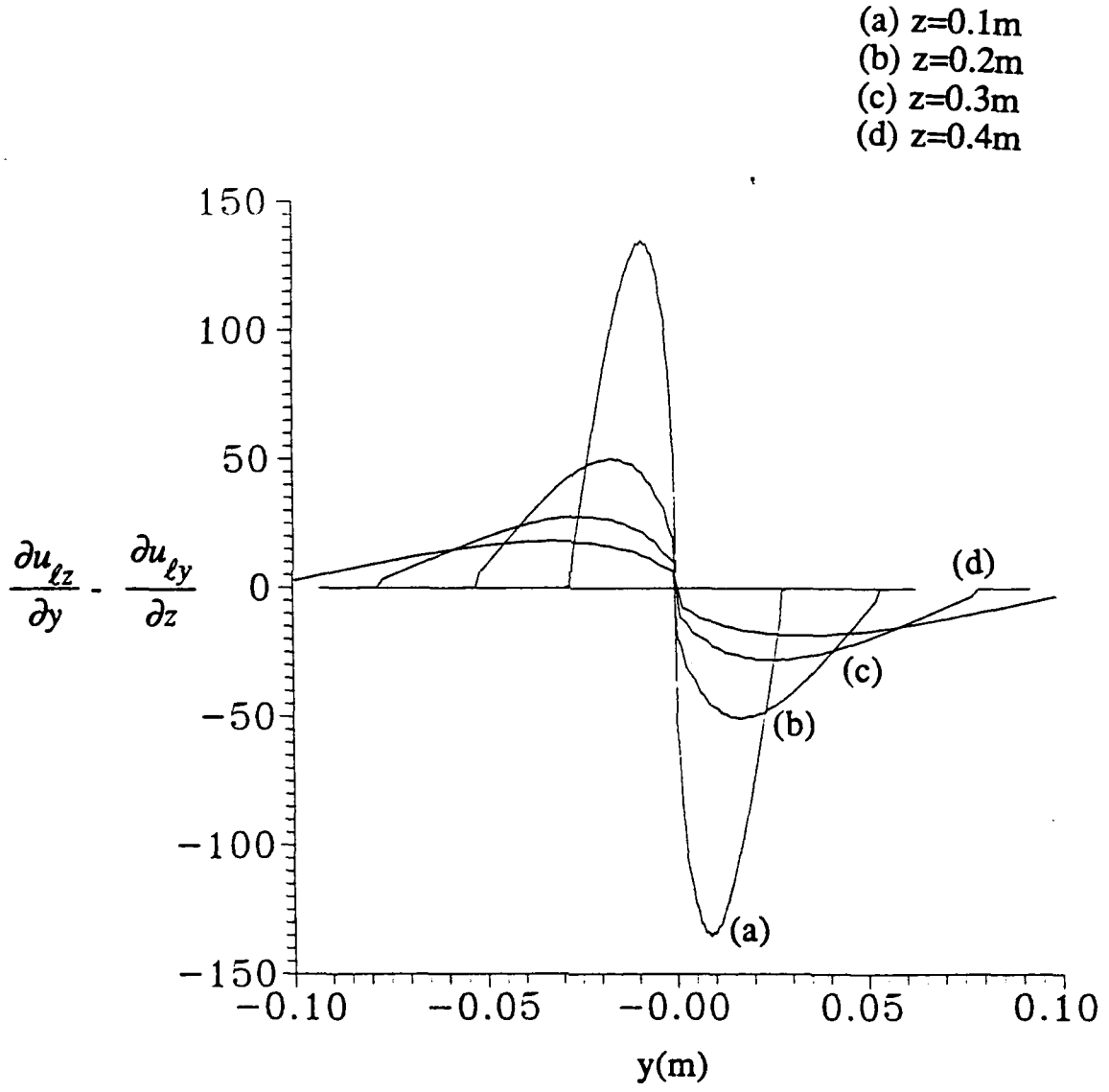

Figure 8: Multiplier for the lift coefficient as a function of the lateral position y for different axial positions z

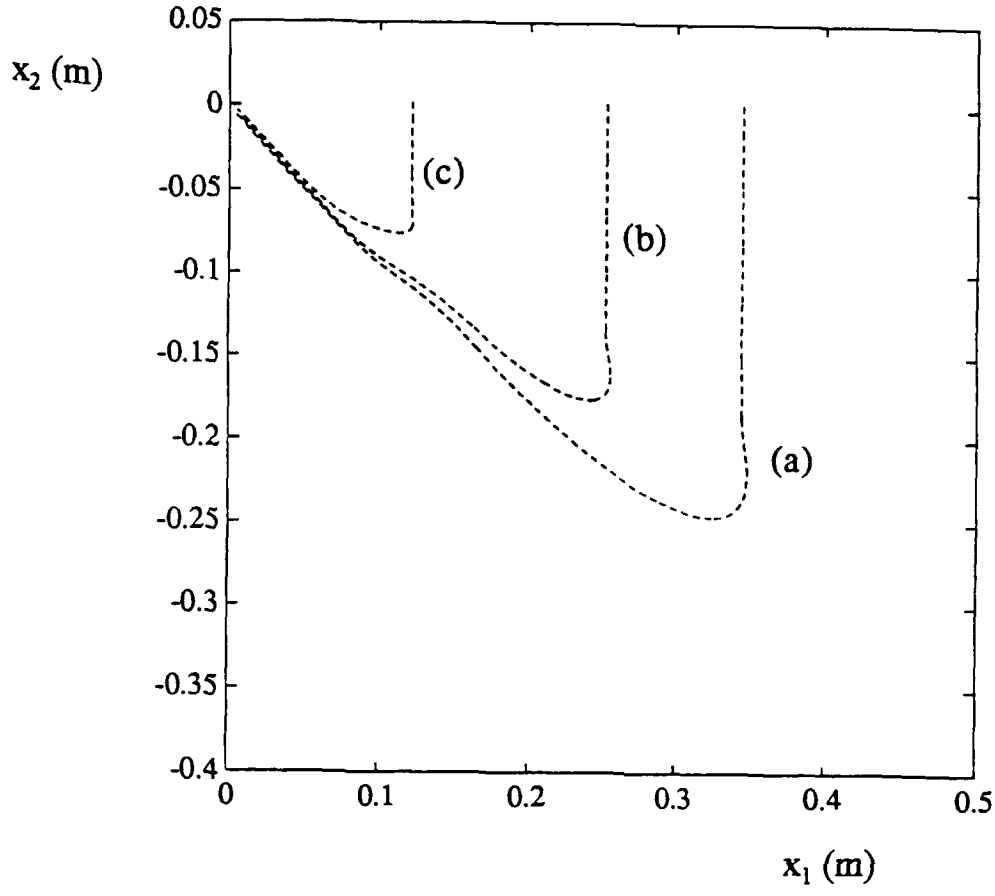

$C_L = 0.5$
$C_{vm} = 0.5$
θ=45°
V=5m/s
R_b=0.002m

Figure 9: Bubble trajectories for the base solution and different initial positions.

(a) y(t=0)=-h/2
(b) y(t=0)=0
(c) y(t=0)=+h/2

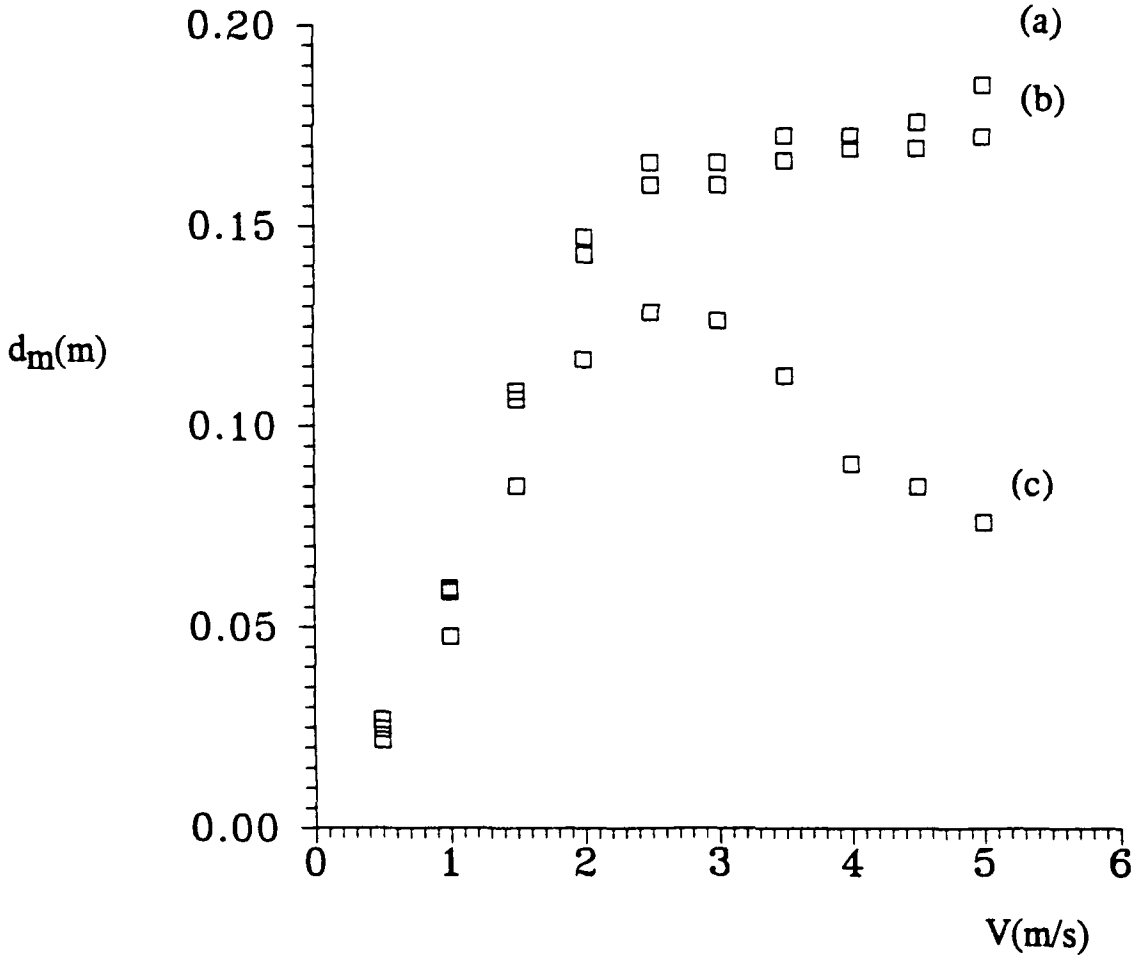

Figure 10: Maximum depth d_m as a function of the jet velocity for different initial positions:

(a) y(t=0)=-h/2
(b) y(t=0)=0
(c) y(t=0)=+h/2

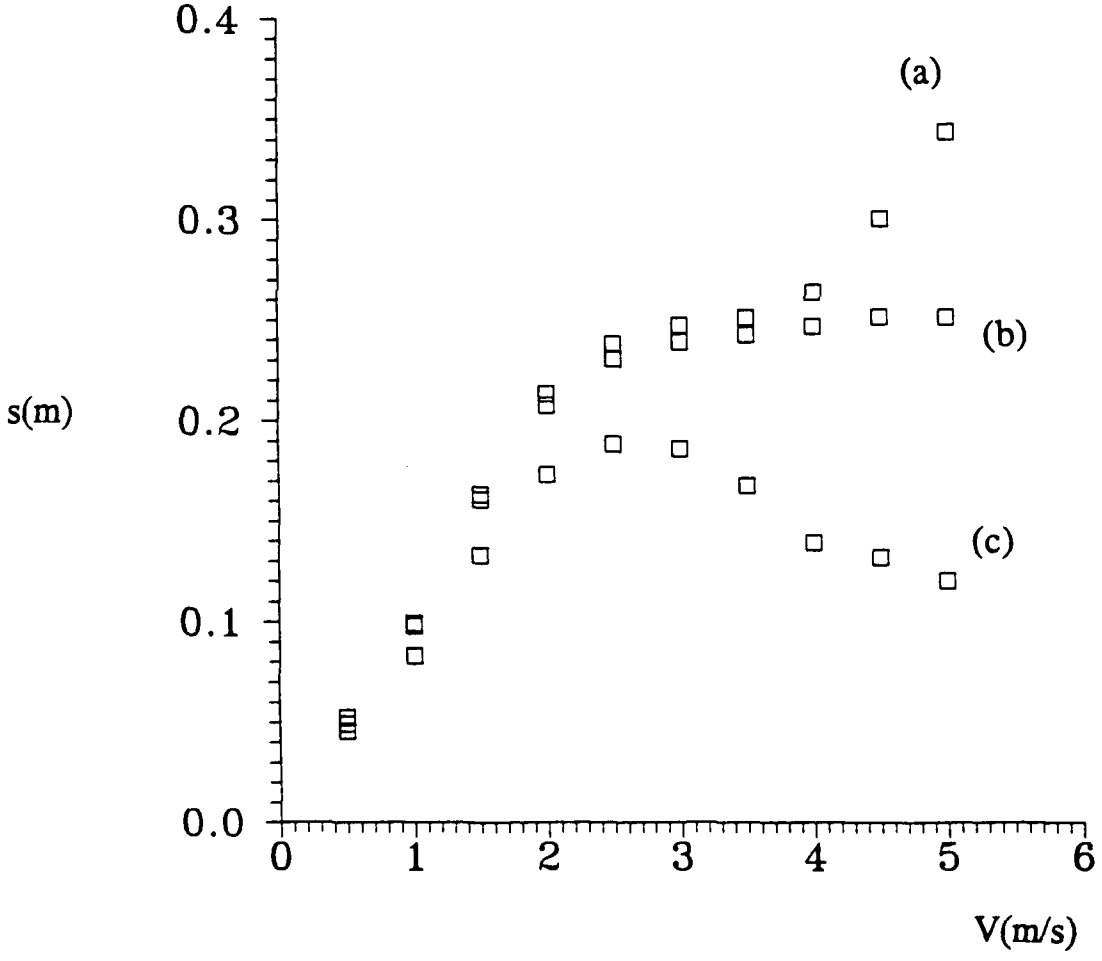

Figure 11: Emergence distance s as a function of the jet velocity for different initial positions:

(a) y(t=0)=-h/2
(b) y(t=0)=0
(c) y(t=0)=+h/2

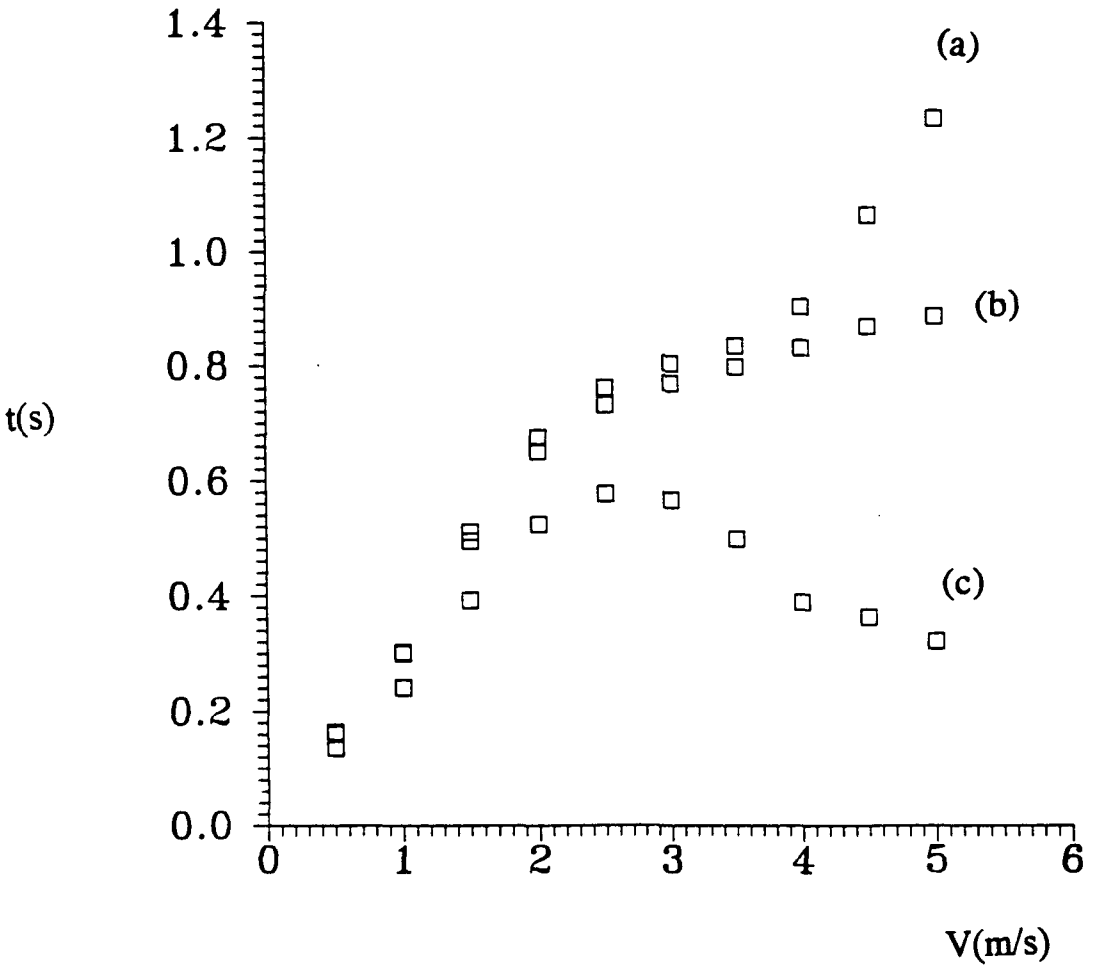

Figure 12: Emergence time t as a function of the jet velocity for different initial positions:

(a) y(t=0)=-h/2
(b) y(t=0)=0
(c) y(t=0)=+h/2

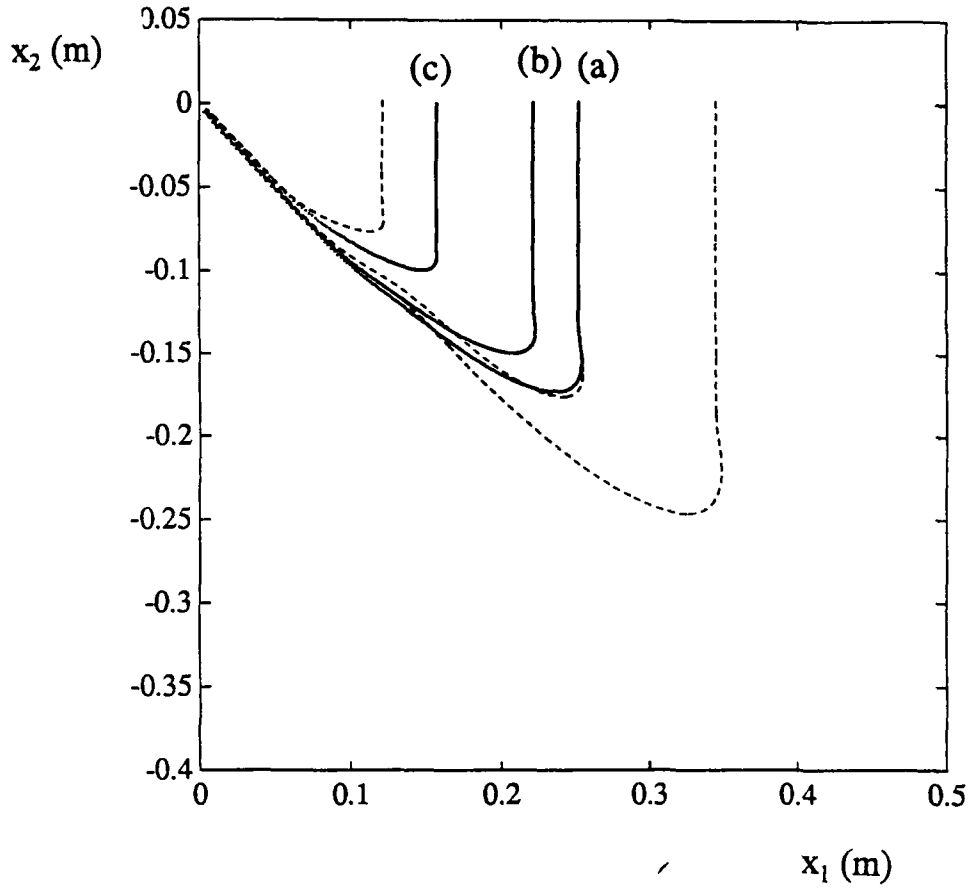

$C_L = 0.5$
$C_{vm} = 0.5$
θ=45°
V=5m/s
R_b=0.002m

Figure 13: Bubble trajectories for C_L=0.25 and different initial positions
(a) y(t=0)=-h/2
(b) y(t=0)=0
(c) y(t=0)=+h/2
The dashed lines are the base solutions

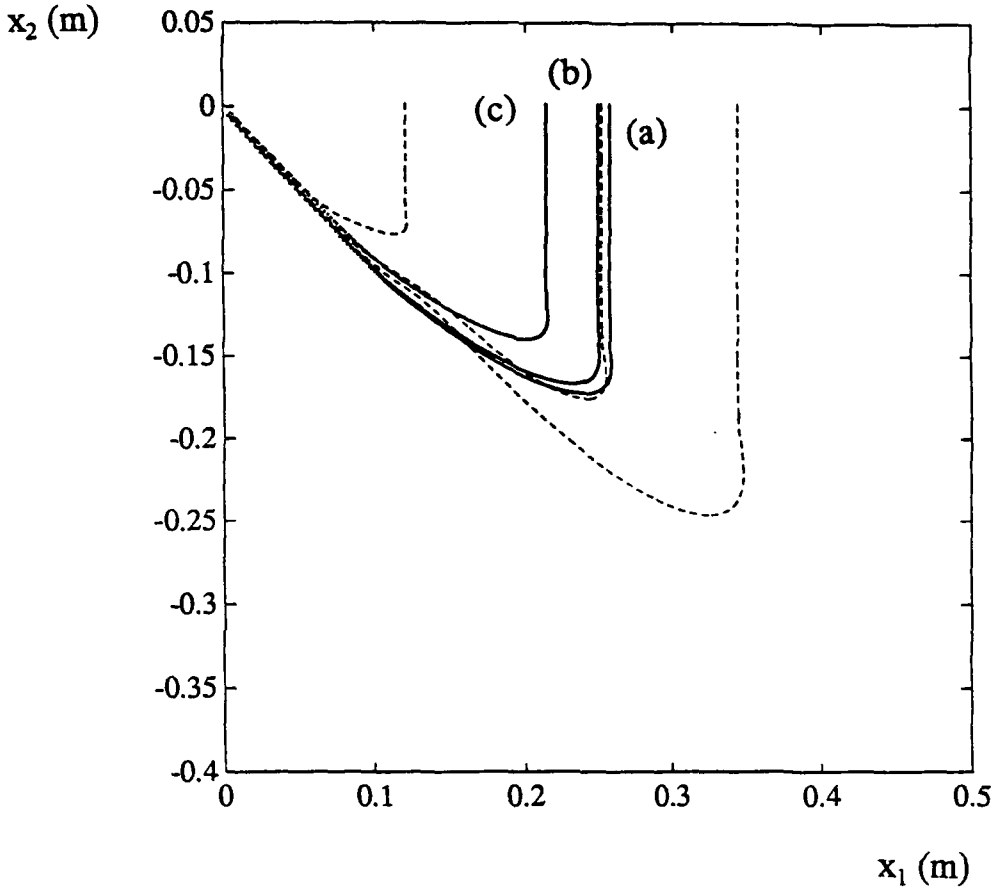

$C_L = 0.5$
$C_{vm} = 0.5$
$\theta=45°$
V=5m/s
R_b=0.002m

Figure 14: Bubble trajectories for C_L=0 and different initial positions
(a) y(t=0)=-h/2
(b) y(t=0)=0
(c) y(t=0)=+h/2
The dashed lines are the base solutions

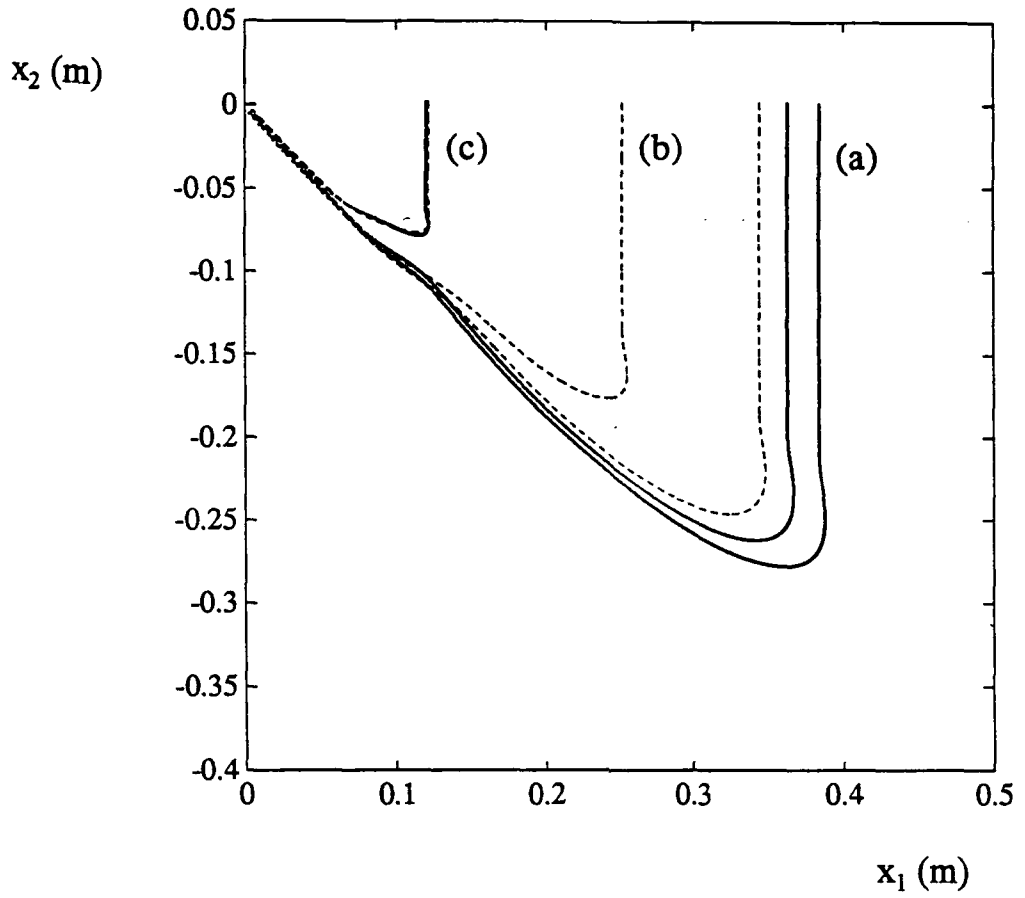

$C_L = 0.5$
$C_{vm} = 0.4$
$\theta = 45°$
V=5m/s
R_b=0.002m

Figure 15: Bubble trajectories for C_{vm}=0.4 and different initial positions
(a) y(t=0)=-h/2
(b) y(t=0)=0
(c) y(t=0)=+h/2
The dashed lines are the base solutions ($C_{vm} = 0.5$)

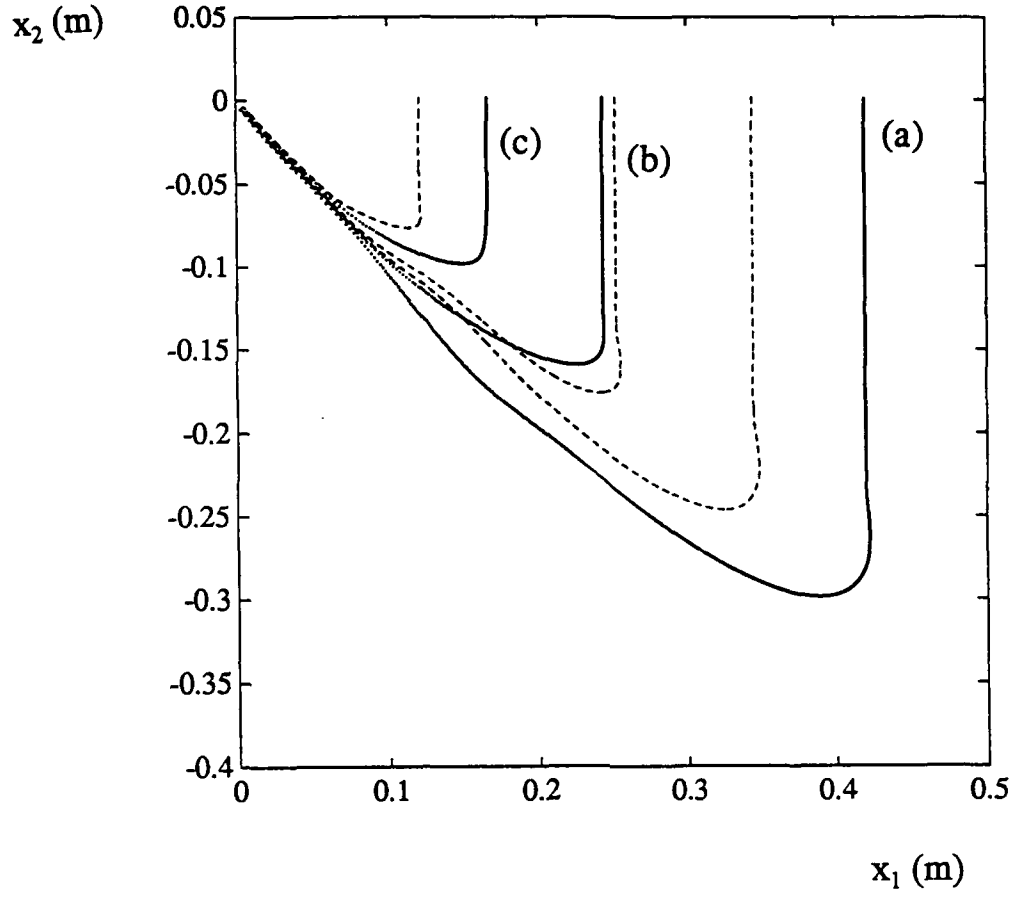

$C_L = 0.5$
$C_{vm} = 1.0$
θ=45°
V=5m/s
R_b=0.002m

Figure 16: Bubble trajectories for C_{vm}=1.0 and different initial positions
(a) y(t=0)=-h/2
(b) y(t=0)=0
(c) y(t=0)=+h/2
The dashed lines are the base solutions ($C_{vm} = 0.5$)

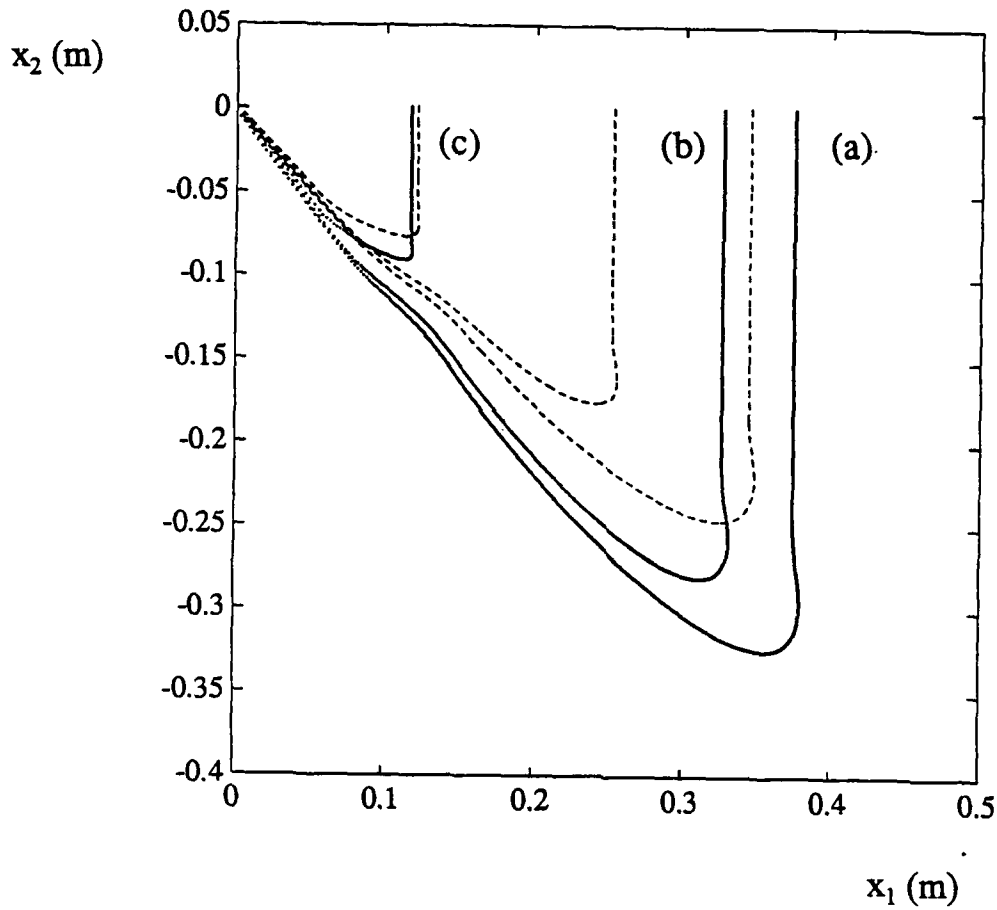

$C_L = 0.5$
$C_{vm} = 0.5$
$\theta=40°$
V=5m/s
R_b=0.002m

Figure 17: Bubble trajectories for $\theta=40°$ and different initial positions
(a) y(t=0)=-h/2
(b) y(t=0)=0
(c) y(t=0)=+h/2
The dashed lines are the base solutions ($\theta=45°$)

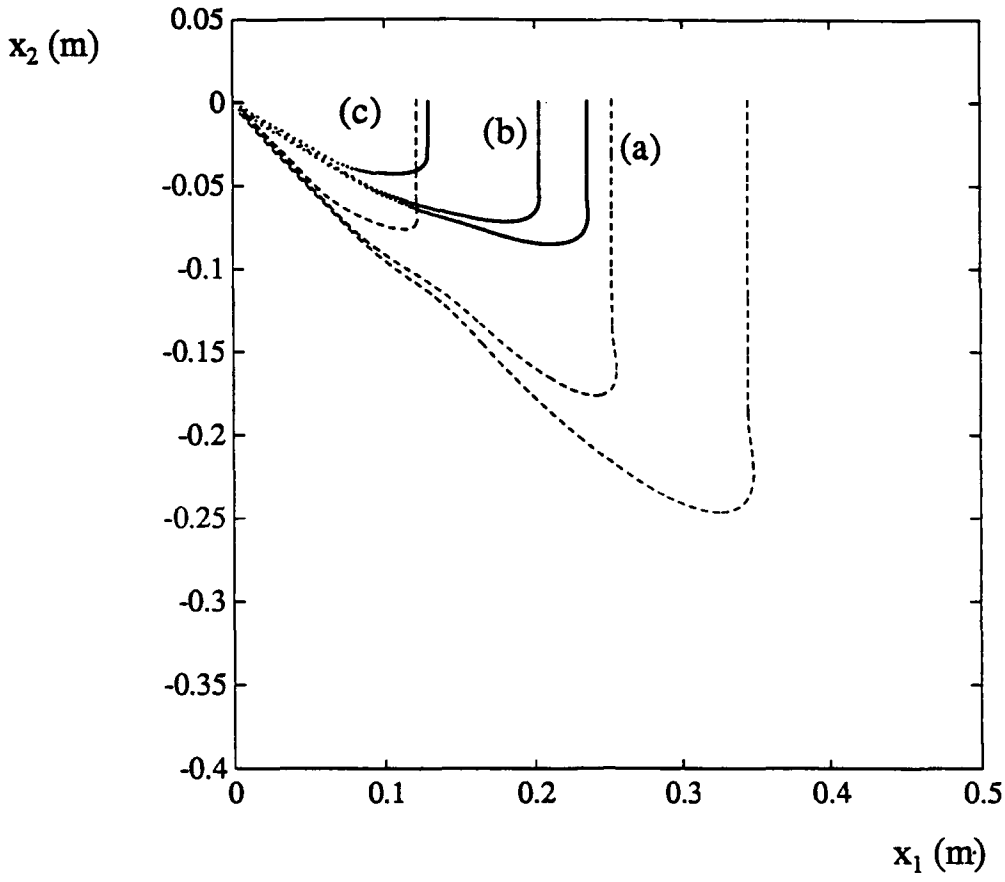

$C_L = 0.5$
$C_{vm} = 0.5$
$\theta=60°$
V=5m/s
R_b=0.002m

Figure 18: Bubble trajectories for $\theta=60°$ and different initial positions
(a) y(t=0)=-h/2
(b) y(t=0)=0
(c) y(t=0)=+h/2
The dashed lines are the base solutions ($\theta=45°$)